

Design and Optimization of Low-thrust Orbit Transfers Using Q-law and Evolutionary Algorithms

Seungwon Lee, Paul von Allmen, Wolfgang Fink, Anastassios Petropoulos, and Richard Terrile
Jet Propulsion Laboratory, California Institute of Technology, Pasadena, CA 91109, USA
818-393-7720
Seungwon.Lee@jpl.nasa.gov

Abstract— Future space missions will depend more on low-thrust propulsion (such as ion engines) thanks to its high specific impulse. Yet, the design of low-thrust trajectories is complex and challenging. Third-body perturbations often dominate the thrust, and a significant change to the orbit requires a long duration of thrust. In order to guide the early design phases, we have developed an efficient and efficacious method to obtain approximate propellant and flight-time requirements (i.e., the Pareto front) for orbit transfers. A search for the Pareto-optimal trajectories is done in two levels: optimal thrust angles and locations are determined by Q-law, while the Q-law is optimized with two evolutionary algorithms: a genetic algorithm and a simulated-annealing-related algorithm. The examples considered are several types of orbit transfers around the Earth and the asteroid Vesta. The optimized Q-law leads to a decent Pareto front which contains the optimal solutions found with other trajectory optimization algorithms. At the same time, the decent Pareto front is obtained within a few hours of computation time. It is both the high optimization quality and the high computational efficiency that make our method attractive as a guiding tool for the early design phases.

TABLE OF CONTENTS

- 1 INTRODUCTION
- 2 Q-LAW
- 3 Q-LAW OPTIMIZATION WITH GA AND SA
- 4 ORBIT-TRANSFER RESULTS
- 5 CONCLUSIONS
- 6 ACKNOWLEDGMENTS
- 7 APPENDIX

1. INTRODUCTION

Future missions DAWN and JIMO will use electric propulsion for the inter-planetary cruise and orbital operations. The control of the low-thrust-driven spacecraft poses a new, challenging design problem. Third-body perturbations often dominate the thrust, and a significant change to the orbit requires a long duration of thrust. With the aim of providing rapid estimates of propellant requirements and flight times for

low-thrust orbit transfers, a control law called Q-law was developed by Petropoulos [1]. It has been demonstrated that the Q-law with a reasonable set of parameters efficiently finds approximate Pareto-optimal solutions (i.e., a propellant-optimal solution for a given flight time or a flight-time-optimal solution for a given propellant requirement) [1][2]. On the other hand, it is also suggested from a grid sampling of the Q-law parameters that a better solution can be found if optimal Q-law parameters are chosen [2]. Finding an optimal set of the Q-law parameters for all possible orbit transfers is analytically impossible and can be computationally expensive without good heuristic algorithms. There is no guarantee that one set of the internal parameters is superior for all types of orbit transfers. It is also not expected that one particular set is superior for all propellant requirements and flight times of a specific orbit transfer. In this paper, we demonstrate that a genetic algorithm and a simulated-annealing-related algorithm efficiently optimize the Q-law parameters, and thus improve an estimation for propellant-mass and flight-time requirements for various orbit transfers.

2. Q-LAW

Q-law was developed by Petropoulos [1] in order to provide good initial guesses for propellant-optimal low-thrust orbit transfers. The Q-law determines when and at what angles to thrust based on the proximity function termed Q . The function Q judiciously quantifies the proximity of the osculating orbit to the target orbit. We will describe the expression of the function Q in the next paragraph. In the Q-law, the central body is modeled as a point mass, and no perturbing forces are considered.

The Q-law consists of two main control rules. 1) At any point on the orbit transfer, the Q-law chooses thrust angles which reduce Q the most. 2) The Q-law determines whether to thrust or coast according to a given thrust effectivity threshold $\eta_{cut} = [0, 1]$ as follows:

$$\text{thrust,} \quad \text{if } \frac{\min_{\alpha, \beta} \dot{Q}}{\min_{\alpha, \beta, \theta} \dot{Q}} \geq \eta_{cut} \quad (1)$$

$$\text{coast,} \quad \text{if } \frac{\min_{\alpha, \beta} \dot{Q}}{\min_{\alpha, \beta, \theta} \dot{Q}} < \eta_{cut}, \quad (2)$$

where \dot{Q} is the time rate of change of Q , α and β are thrust angles (more specifically, azimuthal and polar angles of the thrust with the pole being given by the osculating orbital an-

gular momentum), and θ is the true anomaly of the osculating orbit. $\min_{\alpha,\beta} \dot{Q}$ is the minimum of \dot{Q} over α and β at a given θ , whereas $\min_{\alpha,\beta,\theta} \dot{Q}$ is the minimum of \dot{Q} over α , β , and θ . Thus, η_{cut} is a handle to control the effectivity of the trust. In general, a larger η_{cut} leads to a smaller propellant mass and a longer flight time.

The function Q , which serves as a candidate Lyapunov function in the Q-law, is defined as follows:

$$Q = (1 + W_P P) \sum_{\alpha} W_{\alpha} S_{\alpha} \left[\frac{d(\alpha, \alpha_T)}{\dot{\alpha}_{xx}} \right]^2 \quad (3)$$

for $\alpha = a, e, i, \omega, \Omega$.

The five orbital elements (α) are the semimajor axis (a), eccentricity (e), inclination (i), argument of periapsis (ω), and longitude of the ascending node (Ω); W_P and the W_{α} are scalar weights greater than or equal to zero; the subscript T denotes the target orbit element value (without subscript, the osculating value is indicated); $\dot{\alpha}_{xx}$ denotes the maximum over thrust direction and over true anomaly on the osculating orbit of the rate of change of the orbit element (due to thrust). The analytical expressions for $\dot{\alpha}_{xx}$ are available [1]; P is a penalty function; S_{α} is a scaling function; and $d(\alpha, \alpha_T)$ is a distance function. The penalty function is used in the present paper to enforce minimum-periapsis-radius constraints and takes the form

$$P = \exp \left[k \left(1 - \frac{r_p}{r_{p\text{min}}} \right) \right] \quad (4)$$

where k is a scalar, r_p is the osculating periapsis radius, and $r_{p\text{min}}$ is near or equal to the lowest permissible value of r_p . The scaling function is used primarily to prevent non-convergence to the target orbit and takes the form

$$S_{\alpha} = \begin{cases} \left[1 + \left| \frac{a - a_T}{m a_T} \right|^n \right]^{\frac{1}{n}} & \text{for } \alpha = a \\ 1 & \text{for } \alpha = e, i, \omega, \Omega \end{cases} \quad (5)$$

where m , n , and r are scalars. The distance function is defined as

$$d(\alpha, \alpha_T) = \begin{cases} \alpha - \alpha_T & \text{for } \alpha = a, e, i \\ \cos^{-1}[\cos(\alpha - \alpha_T)] & \text{for } \alpha = \omega, \Omega \end{cases} \quad (6)$$

where the principal value, namely $[0, \pi]$, is used for the arc cosine. The peculiar form of the distance function for ω and Ω is used because it provides an angular measure of the distance between two positions on a circle using the ‘‘short way round’’ the circle, because it is differentiable with respect to α [except when $d(\alpha, \alpha_T) = \pi$], and because the sign of the derivative indicates whether α leads or lags α_T based on the short way round.

As shown above, the Q-law specifies the general form of the proximity function Q and the general rules for optimal thrust angles and thrust locations. However, the Q-law involves a set of internal parameters that needs to be determined by a mission designer. The set is composed of $\{\eta_{\text{cut}}, W_a, W_e, W_i, W_{\omega}, W_{\Omega}, W_P, m, n, r, r_{p\text{min}}, k\}$.

3. Q-LAW OPTIMIZATION WITH GA AND SA

Mathematically, the Q-law parameter optimization problem is expressed as

$$\begin{aligned} \text{minimize } \mathbf{y} &= \{t_f(\mathbf{x}), m_p(\mathbf{x})\} \in \mathbf{Y}, \\ \text{where } \mathbf{x} &= \{W_a, W_e, W_i, W_{\omega}, W_{\Omega}, W_P, \\ &\quad m, n, r, r_{p\text{min}}, k, \eta_{\text{cut}}, \theta_i\} \in \mathbf{X}. \end{aligned} \quad (7)$$

Here, \mathbf{x} is the Q-law parameter vector, \mathbf{y} the objective vector given by required flight time (t_f) and required propellant mass (m_p) for a given orbit transfer, \mathbf{X} the decision space, and \mathbf{Y} the objective space. We add one more parameter to the decision space: the initial true anomaly θ_i which is not a Q-law parameter *per se* but a mission-design parameter. One decision vector \mathbf{x}_i leads to one candidate trajectory with a final flight time and a consumed propellant mass, that is an objective vector \mathbf{y}_i . In the following paragraphs, we will describe how the optimization problem is solved with two evolutionary algorithms: a genetic algorithm and a simulated-annealing algorithm.

Genetic Algorithm

Genetic algorithms (GA), first introduced by John Holland and his colleagues [3], are search algorithms based on the mechanics of natural selection and sexual reproduction. GAs are theoretically and empirically proven to provide robust search in complex spaces. Furthermore, they are not fundamentally limited by restrictive assumptions about the search space such as continuity and existence of derivatives.

The standard GA proceeds as follows. A possible solution of a given problem is encoded as a finite string of symbols, known as the genome. An initial population of the possible solutions called individuals is generated at random or heuristically. Every evolutionary step, known as a generation, the individuals in the current population are decoded and evaluated according to some predefined quality criterion, referred to as the fitness. To form the next generation, parents are selected according to their fitness. Many selection procedures are currently in use, one of the simplest being Holland’s original fitness-proportionate selection, where individuals are selected with a probability proportional to their relative fitness. This ensures that the expected number of times an individual is chosen is approximately proportional to its relative performance in the population. Thus, high-fitness individuals stand a better chance of reproducing, while low-fitness ones are more likely to disappear.

The parent selection process is followed by genetically-inspired operators to form offsprings. The most well known operators are crossover and mutation. Crossover is performed with probability p_{cross} between two selected parents, by exchanging parts of their genomes to form two offsprings; in its simplest form, substrings are exchanged after a randomly selected crossover point. This operator tends to enable the evolutionary process to move toward ‘‘promising’’ regions of the search space. The mutation operator is introduced to prevent

Table 1. Initial and final orbit elements, thrust characteristics, spacecraft initial masses, and central bodies associated with the orbit transfers studied in this paper. The orbit elements are given by the semimajor axis (a), the eccentricity (e), inclination (i), argument of periapsis (ω), and longitude of the ascending node (Ω). Note that the true anomaly (θ) is left free for both the initial and final orbit.

Case	Orbit	a (km)	e	i (degree)	ω (degree)	Ω (degree)	Thrust (N)	Specific Impulse (s)	Initial Mass (kg)	Central Body
A	Initial	7000.00	0.010	0.050	0.0	0.00	1	3100	300	Earth
	Target	42000.00	0.010	free	free	free				
B	Initial	24505.90	0.725	7.050	0.0	0.00	0.350	2000	2000	Earth
	Target	42165.00	0.001	0.050	free	free				
C	Initial	9222.70	0.200	0.573	0.0	0.00	9.3	3100	300	Earth
	Target	30000.00	0.700	free	free	free				
D	Initial	944.64	0.015	90.060	156.9	-24.60	0.0045	3045	950	Vesta
	Target	401.72	0.012	90.010	free	-40.73				
E	Initial	24505.90	0.725	0.060	180.0	180.00	2	2000	2000	Earth
	Target	26500.00	0.700	116.000	270.0	180.00				

premature convergence to local optima by randomly sampling new points in the search space with some probability p_{mut} . Genetic algorithms are stochastic iterative processes that are not guaranteed to converge. The termination condition may be specified as some fixed, maximal number of generations or as the attainment of an acceptable fitness level.

We apply the standard GA to optimize the Q-law parameters. While the standard GA is closely followed, a ranking scheme known as nondominated sorting is added in the process of fitness assignment [10]. Optimizing the Q-law parameters is a type of multi-objective optimization problems, because both propellant masses and flight times need to be minimized. In such a problem, there may not exist one solution that is best with respect to all objective. Therefore, the goal of the multi-objective optimization problem is to determine the trade-off surface, which is a set of nondominated solution points, known as Pareto-optimal or non-inferior solutions. A conventional way to solve multi-objective problems is to transform the original problem in a single-objective one, by weighting the objectives with a weight vector. However, this process tends to lead to a subgroup of Pareto-optimal solutions that is sensitively chosen to the weight vector used in the weighting process. In contrast, the nondominated sorting encourages equally all nondominated solutions to survive. The nondominated sorting genetic algorithm (NSGA) is proven to be superior [4] to other multi-objective evolutionary algorithms such as the vector evaluated genetic algorithm (VEGA) [5], the niched Pareto genetic algorithm (NPGA) [6], and the multi-objective genetic algorithm (MOGA) [7].

The nondominated sorting proceeds as follows. First, the nondominated individuals in the current population are identified, as described in the Appendix. Then, the same fitness value is assigned to all the individuals constituting the first

nondominated front. Afterwards, the individuals are ignored temporarily, and the rest of the population is processed in the same way to identify the nondominated individuals. A fitness value that is smaller than the previous one is assigned to all the individuals belonging to the second nondominated front. This process continues until the whole population is classified into nondominated fronts.

Simulated Annealing

Simulated annealing (SA) is a widely used and well-established optimization technique especially for high-dimensional configuration spaces [8][9]. The goal is to minimize an energy function E (in our case, the required flight time and propellant mass), which is a function of N variables (in our case, the Q-law parameters), with N being a large number. The minimization is performed by randomly changing the value of one or more of the N variables and reevaluating the energy function E . Two cases can occur: 1) the change in the variable values results in a new, lower energy function value; or 2) the energy function value is higher or unchanged. In the first scenario the new set of variable values is stored and the change accepted. In the second scenario, the new set of variable values is only stored with a certain likelihood (Boltzmann probability, including an annealing temperature). This ensures that the overall optimization algorithm does not get stuck in local minima too easily (greedy downhill optimization). The annealing temperature directly influences the Boltzmann probability by making it less likely to accept an energetically unfavorable step, the longer the optimization lasts (cooling schedule). Then the overall procedure is repeated until the annealing temperature has reached its end value or a preset number of iterations have been exceeded.

We apply a derivative of the canonical SA algorithm to the

low-thrust-trajectory optimization problem, by replacing the Boltzmann probability acceptance with an energy threshold acceptance: each configuration with an energy $E < E_{\min} + E_{\text{threshold}}$ will be automatically accepted, with $E_{\text{threshold}}$ oscillating between to preset boundaries (“simulated reheating and cooling”).

4. ORBIT-TRANSFER RESULTS

The parameters of the Q-law are optimized by GA and SA for five different types of orbit transfers. Table 1 lists the initial and final orbit elements, thrust characteristics, spacecraft initial mass, and central bodies associated with the five orbit transfers termed case A, B, C, D, and E. The Pareto fronts obtained with the optimized Q-law are compared with those obtained with the normal (unoptimized) Q-control law and available solutions generated by other optimization tools.

The normal Q-law uses $W_{\mathcal{A}} = 1$ for orbit elements with target values, $W_{\mathcal{A}} = 0$ for orbit elements without target values, and $m = 3, n = 4, r = 2$ for the scaling function of the semimajor axis a . The penalty function to enforce minimum-periapsis-radius constraints is applied only for case D and E orbit transfers. The penalty function of the normal Q-law uses $W_p = 1, k = 100$, and $r_{p\min} = 300$ for case D and $r_{p\min} = 6578$ for case E. The Pareto front of the normal Q-law is acquired by varying the thrust effectivity threshold $\eta_{\text{cut}} = [0, 1]$ and the initial true anomaly $\theta_i = [0, 2\pi]$.

The GA optimization uses the following GA parameters: the population size $N_p = 1000$ for case A, B, C and $N_p = 2000$ for case D and E, the number of generations $N_g = 100$, the population replacement rate $p_r = 0.1$, the crossover probability $p_c = 0.8$, the mutation probability $p_m = 0.3$. The relatively high mutation rate is chosen to ensure the diversity of the population. Each Q-law parameter is represented as a real-valued gene. The fitness of each individual is assigned according to the nondominated sorting as described in Sec. ???. Possible parents are selected by tournament (i.e., randomly pick two individuals and choose the one who is better fitted between the two). The crossover is performed by choosing one point in the gene string at which the two strings are crossed. The mutation is performed by randomly choosing a gene in the string according to the mutation probability and resetting the gene randomly within a given range.

Case A Orbit Transfer

Case A is a simple coplanar, circle-to-circle orbit transfer from low Earth orbit to geostationary orbit. No periapsis constraint is imposed during the transfer, as the natural dynamics do not decrease the periapsis altitude. Figure 1 shows the Pareto front obtained by the normal Q-law and the optimized Q-law. Note that each solution in the Pareto front for the optimal Q-law is obtained with a different set of Q-law parameters. As shown Fig. 1, the GA/SA Pareto front dominates the Pareto front given by the normal Q-law.

The Pareto-optimal solutions found by GA and SA are compared with two available analytical solutions: Edelbaum transfer and Hohmann transfer. Edelbaum transfer provides the lower limit for the required flight time [11], while Hohmann transfer sets the lower limit for the required propellant mass. When the Q-law optimized with GA/SA is used, the flight-time-optimal solution is about 0.04 days away from the lower limit of the flight time, and the propellant-optimal solution is about 0.04 kg away from the lower limit of the propellant mass. In contrast, the flight-time optimal solution found by the normal Q-law is 0.11 days away, and the propellant-optimal solution is 0.81 kg away. This comparison clearly shows that the optimization of the Q-law with GA/SA leads to substantial improvement in the estimation of the “true” Pareto front. In particular, the Edelbaum transfer uses a limited thrust, thus can be compared with our low-thrust trajectory solutions in terms of both flight time and propellant mass. Our solution that is closest to the Edelbaum solution in the objective space (propellant-mass vs flight-time) is about 0.2 days and 0.002 kg away from the Edelbaum solution. The Hohmann transfer assumes a unlimited thrust, thus the direct comparison of the flight time of the Hohmann transfer with that of our low-thrust (assumes a limited thrust) transfer is inappropriate.

One of the critical limitations of the normal Q-law is that the particularly chosen Q-law parameters excludes a subgroup of Pareto-optimal solutions. The problem appears in Case A orbit transfer. As shown in Fig. 1, the normal Q-law provides only two families of the Pareto-optimal solutions: one for short flight times ($14 < t_f < 17$) and the other for long flight times ($t_f > 140$). No solutions are found for the intermediate flight times ($17 < t_f < 140$). In contrast, the GA-optimized Q-laws lead to the Pareto-optimal solutions in a wide range of flight times without a significant gap. This indicates that some Q-law parameters besides η_{cut} and θ_i strongly affect the trajectories to be taken.

To show which parameters are important in determining the trajectory pattern, we investigate a correlation between the optimal parameters and the flight time (or the propellant mass). While other Q-law parameters do not show much correlation, the optimal W_e/W_a and η_{cut} show a strong correlation with the flight time, as shown in Figure 2. In other words, for a given set of Q-law parameters the resulting trajectory pattern is determined mainly by W_e/W_a and η_{cut} . The trajectory is less sensitive to other Q-law parameters. For example, the trajectory with flight time 50 days can be found only with $W_e/W_a = 0.81$ and $\eta_{\text{cut}} = 0.84$, while the rest of Q-law parameters can vary widely. This sensitivity/correlation analysis between the Q-law parameters and the resulting trajectory suggests that the Q-law can be effectively optimized by varying only W_e/W_a and η_{cut} .

We present a few typical trajectories for flight-time optimal solutions, propellant-optimal solutions, and intermediate-flight-time solutions found by the optimized Q-law. The

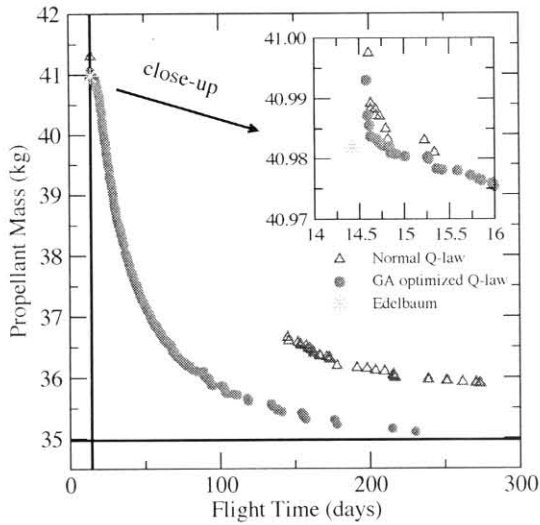


Figure 1. Case A: Trade-off between propellant mass and flight time. The Pareto fronts generated by the normal Q-law and the GA optimized Q-law are plotted in comparison with the lower bounds (solid lines) of the required flight time and propellant mass given by the Edelbaum and Hohman transfers, respectively.

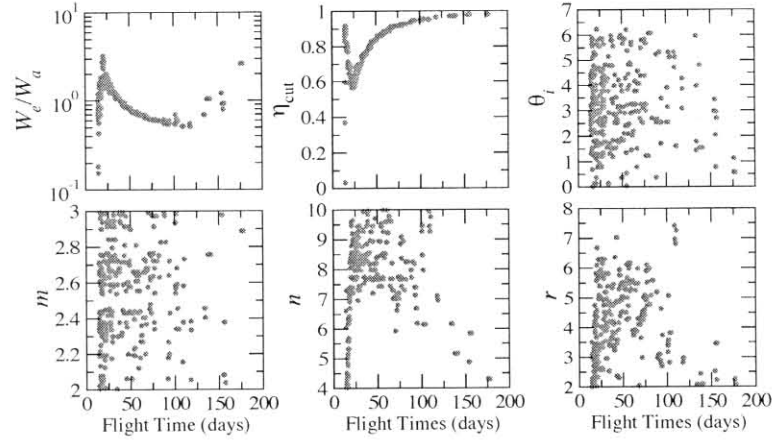


Figure 2. Case A: Optimal Q-law parameters found by GA with respect to flight time. There is a strong correlation between W_e/W_a and the flight time, and between η_{cut} and the flight time, while other Q-law parameters show a weak correlation.

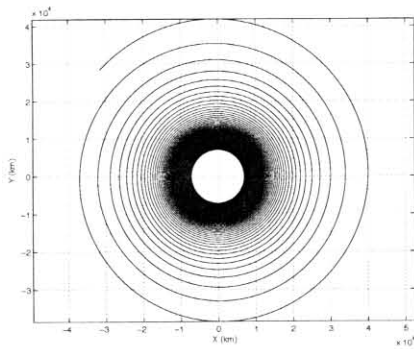


Figure 3. Case A: flight-time-optimal trajectory. It is roughly a circular spiral, increasing the semimajor axis while maintaining the eccentricity close to zero. This is close to the Edelbaum transfer.

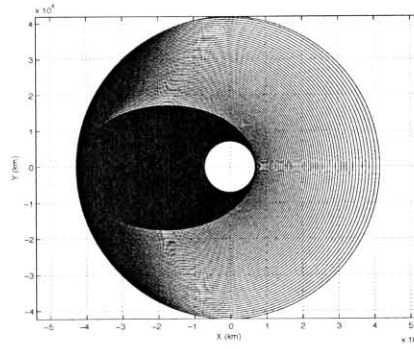


Figure 4. Case A: propellant-optimal trajectory. In the first stage of the trajectory, the same periaapsis is maintained while the apoapsis becomes supersynchronous to the target circular orbit. In the second stage, only the periaapsis is increased while the apoapsis is kept constant. This is a type of the Hohman transfer with a limited thrust.

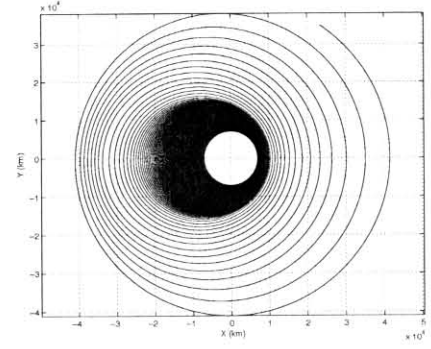


Figure 5. Case A: intermediate-flight-time trajectory. It is a mixed trajectory between the flight-time optimal trajectory and the propellant-optimal trajectory. The trajectory initially increases both the eccentricity and the semimajor axis, and later reduces the eccentricity while continuing to increase the semimajor axis.

flight-time-optimal trajectory is roughly a circular spiral, increasing the semimajor axis while maintaining the eccentricity close to zero, as shown in Figure 3. The propellant-optimal trajectory takes a quite different form, maintaining the same periaapsis until the apoapsis becomes supersynchronous, and then increasing the periaapsis to the target value, as shown in Figure 4. As expected, the intermediate-flight-time trajectory, shown in Figure 5, is a hybrid between the flight-time optimal one and the propellant-optimal one, increasing the periaapsis

and apoapsis simultaneously.

Case B Orbit Transfer

Case B is a transfer from a slightly-inclined geostationary transfer orbit to geostationary orbit. Figure 6 shows the trade-off between propellant-mass and flight-time for this transfer. In comparison with the Pareto front generated by the normal Q-law, the improvement of the Pareto front with the Q-law

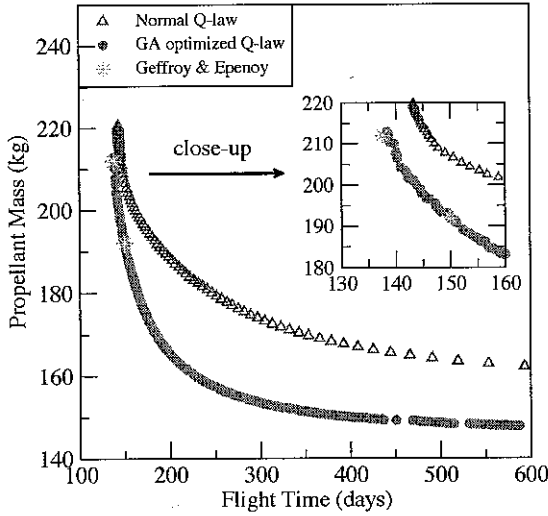


Figure 6. Case B: Trade-off between propellant mass and flight time. The Pareto fronts generated by the normal Q-law and the GA optimized Q-law are plotted in comparison with the Pareto-optimal solutions found by Geffroy and Epenoy using an orbit averaging technique.

optimization is dramatic. A about 5–15% propellant savings is achieved with the optimized Q-law. To verify the quality of the improved Pareto front, we compare it with the two optimal trajectories found by Geffroy and Epenoy using an orbit averaging technique [12]. The inset of Fig. 6 shows that our Pareto-optimal solutions are as good as the solutions found by Geffroy and Epenoy.

A similar analysis about the correlation between Q-law parameters and the resulting solution (flight time and propellant mass) for this transfer is performed, as shown in Figure 7. The dense population of optimal W_a around 10%, optimal W_e around 20%, and W_i around 70% shows that the normal Q-law ($W_a = W_e = W_i$) is not an optimal choice. As expected, the thrust effectivity threshold η_{cut} is the important parameter to control the flight time. Other Q-law parameters (m, n, r) and the initial true anomaly (θ_i) show weak correlation with the flight time, indicating that the parameters are not as critical as W_a, W_e, W_i , and η_{cut} in the Q-law optimization.

Case C Orbit Transfer

Case C is a transfer from a low-eccentricity elliptic orbit to a coplanar, high-eccentricity, larger elliptic orbit. Figure 8 shows the trade-off between propellant mass and flight time for this transfer. The Pareto front for the normal Q-law is obtained by varying the thrust effectivity threshold $\eta_{cut} = [0, 1]$ and the initial true anomaly $\theta_i = [0, 2\pi]$. The Pareto front for the GA optimized Q-law is generated by optimizing $\{W_a, W_e, m, n, r, \eta_{cut}, \theta_i\}$. The GA optimized Q-law provides a better estimation of the Pareto front than the normal Q-law particularly for short flight times. Several solutions found by the optimization tool named Mystic are plotted for comparison. Mystic uses the static/dynamic control algo-

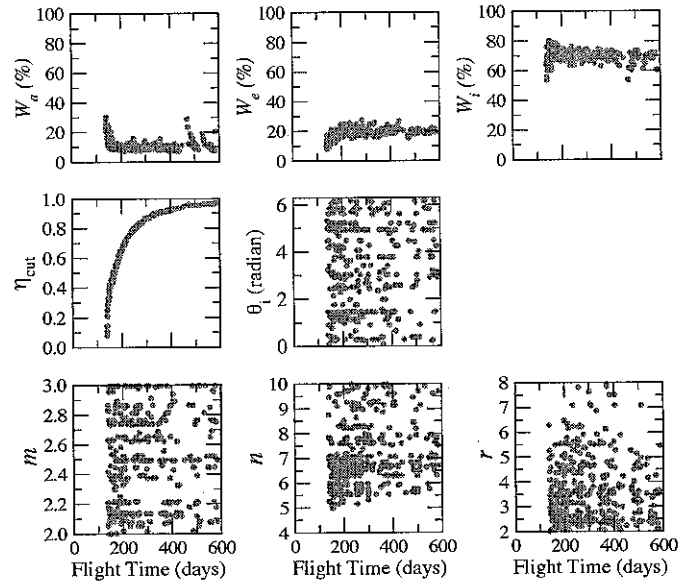


Figure 7. Case B: Optimal Q-law parameters found by GA with respect to flight time. Optimal W_a, W_e, W_i are normalized to make its sum to be 100%.

rithm [13] [14]. The comparison shows that the Pareto front generated by the optimized Q-law is as good as or better than the Mystic solutions.

The optimal Q-law parameters found by GA are plotted with respect to flight time in Fig. 9. The optimal W_e/W_a and η_{cut} are strongly correlated to the flight time, while other Q-law parameters show a weak correlation. Generally, flight-time-optimal solutions have $W_e/W_a > 1$, while propellant-optimal solutions have $W_e/W_a < 1$. This means that the flight-time-optimal solutions emphasize the eccentricity target while the propellant-optimal solutions emphasize the semi-major axis target.

Case D Orbit Transfer

Case D is roughly a circle-to-circle orbit transfer around the asteroid Vesta, involving a small plane change. Figure 10 shows the trade-off between propellant mass and flight time for this transfer. The Pareto front of the normal Q-law is obtained by varying the thrust effectivity threshold $\eta_{cut} = [0, 1]$ and the initial true anomaly $\theta_i = [0, 2\pi]$. The Pareto fronts of the GA optimized Q-law are generated in three different ways: the first Pareto front (GA Q-law I) is obtained by optimizing $\{W_a, W_e, W_i, W_\Omega, \eta_{cut}, \theta_i\}$, the second Pareto front (GA Q-law II) by optimizing $\{W_a, W_e, W_i, W_\Omega, \eta_{cut}, \theta_i, m, n, r\}$, and the third Pareto front (GA Q-law III) by optimizing $\{W_a, W_e, W_i, \eta_{cut}, \theta_i, m, n, r, W_P, r_{pmin}, k\}$. In comparison with the normal Q-law, the GA optimized Q-law improves an estimation of the Pareto front for all the flight times considered. The GA optimized Q-law leads to a propellant mass savings as much as 16%. More promisingly, the Pareto-optimal solutions found by the optimized Q-law are as good

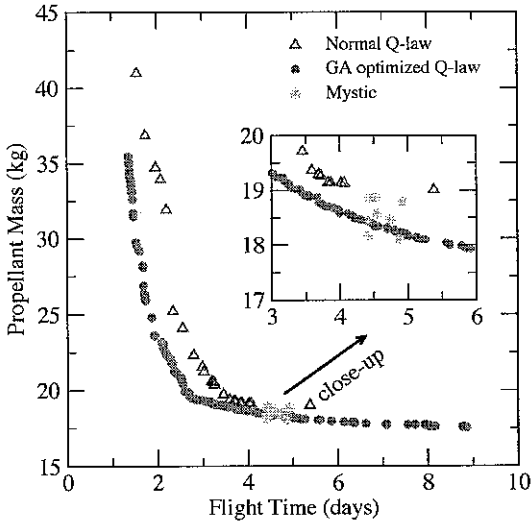


Figure 8. Case C: Trade-off between propellant mass and flight time. The Pareto fronts generated by the normal Q-law and the optimized Q-law are plotted in comparison with several Pareto-optimal solutions found by optimization tool Mystic.

as the solution found by Whiffen using the static/dynamic control algorithm [14] [15].

Among the three GA optimization schemes described above, GA Q-law II and GA Q-law III outperform GA Q-law I but the difference between GA Q-law II and GA Q-law III is insignificant. This result indicates that the trajectory does not depend strongly on $\{W_p, r_{pmin}, k\}$ (the parameters of the penalty function for the minimum periapsis constraint) and thus a decent Pareto front can be obtained by optimizing only $\{W_a, W_e, W_i, \eta_{cut}, \theta_i, m, n, r\}$. The difference between the Pareto fronts generated by GA Q-law I and GA Q-law II (or III) becomes smaller as the flight time becomes longer. This sheds some light on the effect of Q-law parameters m, n, r on the Q-law performance. The parameters m, n, r are introduced for the scaling function in the semimajor axis to ensure the convergence of the trajectory which involves the increase of the semimajor axis. However, the semimajor axis steadily decreases in this orbit transfer indicating no strong need for the scaling function. Therefore, it is preferred to have the parameter set m, n, r that yields a smallest modification to the distance function.

Optimal Q-law parameters found by GA are plotted with respect to flight time in Figure 11. Optimal W_a, W_e, W_i, W_Ω are normalized to make the sum to be 100%. The Q-law optimization shows greater selectivity about $W_a, W_e, W_i, W_\Omega, \eta_{cut}, \theta_i, m, n,$ and r than about $W_p, r_{pmin},$ and k . This explains why the Pareto front generated by GA Q-law II is as good as the Pareto front generated by GA Q-law III, shown in Figure 10. Similar to others, this transfer also shows a strong correlation between η_{cut} and flight time. However, the correlation does not follow a sim-

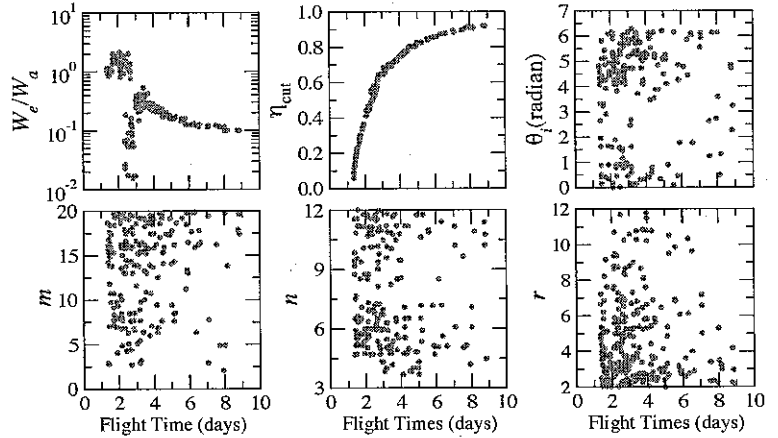


Figure 9. Case C: Optimal Q-law parameters found by GA with respect to flight time. There is a strong correlation between W_e/W_a and the flight time and between η_{cut} and the flight time, while other Q-law parameters show a weak correlation.

ple trend: the larger η_{cut} , the longer flight time. The optimal η_{cut} shows a discontinuity around flight time 60 days. The discontinuity also appears in other optimal Q-law parameters such as W_a, W_e, W_Ω . This indicates that the pattern of the trajectory changes around the flight time.

To understand the cause of the discontinuity of the optimal Q-law parameters, we examine the trajectory of the flight time just below the discontinuity point (T1) and that of the flight time just above the discontinuity point (T2). Figure 12 shows orbit elements as a function of time during the orbit transfer. The two trajectories show a significant difference in the time history of eccentricity, while other orbit elements (a, i, ω, Ω) show a small difference. T1 keeps the eccentricity close to zero all time, but T2 shows the large increase and decrease of the eccentricity during the orbit transfer. This trend is similar to that observed in case A transfer, where the circular spiral trajectory (Edelbaum-type transfer) is flight-time optimal and the elliptic trajectory (Hohmann-type transfer) is propellant optimal. The two types of trajectories can be obtained with the Q-law by either emphasizing the eccentricity target or not. This result is shown in the distribution of the optimal W_e in Figure 11. The optimal W_e is greater for short-flight-time solutions than for long-flight-time solutions.

Case E Orbit Transfer

Case E is a transfer from a geostationary transfer orbit to a retrograde, Molniya-type orbit, involving a large plane change. Figure 13 shows the trade-off between propellant mass and flight time for this transfer. The Pareto front for the normal Q-law is obtained with varying $\eta_{cut} = [0, 1]$ and the initial true anomaly $\theta_i = [0, 2\pi]$. Three Pareto fronts are generated with GA optimization as fol-

lows: the first Pareto front (GA-Q-law I) by optimizing $\{W_a, W_e, W_i, W_\omega, W_\Omega\}$, the second Pareto front (GA Q-law II) by optimizing $\{W_a, W_e, W_i, W_\omega, W_\Omega, m, n, r, \eta_{cut}, \theta_i\}$, and the third Pareto front (GA Q-law III) by optimizing $\{W_a, W_e, W_i, W_\omega, W_\Omega, m, n, r, \eta_{cut}, \theta_i, W_P, r_{pmin}, k\}$. The GA optimized Q-law provides a better estimation of the Pareto front than the normal Q-law for all the flight times considered. The propellant mass savings as much as 30% is obtained with the GA optimized Q-law. Similar to the case D, GA Q-law II and GA Q-law III outperform GA Q-law I, while the difference between GA Q-law II and III is insignificant. This result reflects the degree of the influence of each Q-law parameter on the Q-law performance. The difference between GA Q-law I and GA Q-law II (or III) becomes larger as the flight time increases in opposite to the case D.

Optimal Q-law parameters found by GA are plotted with respect to flight time in Figure 14. The overall distribution of the optimal Q-law parameters shows the greater sensitivity of the Q-law performance to $\{W_a, W_e, W_i, W_\Omega, \eta_{cut}\}$ than to $\{m, n, r, W_P, r_{pmin}, k\}$. The optimal η_{cut} shows a strong correlation with flight time similar to other transfers. A strong preference of relative size order $W_i > W_\Omega > W_a > W_\omega > W_e$ is observed for all flight times.

Case E involves specified changes in all orbit elements, making it the most complicated transfer among the five transfers studied here. We examine how the change of each orbit element interacts with other orbit-element changes. Figure 15 shows the time history of each orbit element for four different Pareto-optimal trajectories found by GA Q-law III. It is commonly observed for all four trajectories that the plane changes (i.e. i, ω, Ω) occurs when the semimajor axis reaches near the maximum values, and the increase of semimajor axis is accompanied by the increase of eccentricity. This behavior stems from the orbit-transfer energetics that the larger apoapsis radius (i.e. larger semimajor axis and larger eccentricity) makes the plane change less costly in terms of propellant.

Figure 15 also shows the general trend of the orbit-element changes with respect to the flight time. In general, the trajectory with a longer flight time involves a larger change of semimajor axis and a late start of plane change. For example, the shortest-flight-time trajectory (the solid line) exhibits the early start of the plane change and the semimajor axis peaked at 50000 km. In contrast, the longest-flight-time trajectory (the line with circles) shows almost zero plane change until the semimajor axis reaches its maximum 100000 km. The difference is directly related to the orbit-transfer energetics that the plane change with a larger apoapsis radius is propellant efficient. The longer flight-time trajectory takes more advantage of the energetics. The top panel of Fig. 15 illustrates the time history of propellant usage during the transfer. The shortest-flight-time trajectory uses propellant with almost a constant rate. The longer-flight-time trajectories use propellant with a lower rate during the first stage of increasing the semimajor axis followed by a higher rate of propellant con-

Table 2. Computation times required to obtain a Pareto front for each orbit transfer. GA computation was performed with 10 processors in parallel, thus required the wall-clock time that is one tenth of the listed computation time.

Orbit Transfer Case	Computation Time (minutes)	
	GA	SA
A	705	
B	800	
C	57	
D	1548	
E	2480	

sumption in the second stage of changing the plane.

Computational Requirement

The computation time required to obtain the Pareto front of each orbit transfer is listed in Table 2. Case C requires a relatively short computation time because the evaluation of each Q-law takes less time due to the short flight time in Case C transfer. Beside Case C, the required computation time is about between 700 to 2500 minutes. For Case A, B, and C, the GA computation evaluates 1100 sets of Q-law parameters, while for Case D and E it evaluates 2200 sets of Q-law parameters. Therefore, the time to evaluate one set of Q-law parameters (equivalently to obtain a candidate trajectory and to assign its fitness) is only about 1 minute in average.

In addition to the efficient evaluation of candidate Q-laws/trajectories, GA is straightforward to perform parallel computation thanks to the independent evaluation of each candidate Q-law/trajectory in population. The parallel computation significantly reduces the wall-clock time for a given computational work. For this work, we take advantage of the easy parallelism of GA. The GA computation was performed with 10 processors in parallel, thus required the wall-clock time that is one tenth of the computation time listed in Table 2. It is the short wall-clock time (70 – 250 minutes) that makes our optimization method attractive as a guiding tool for the early stage of mission design where many possible scenarios need to be considered. It is important to note that our method provides a decent Pareto front (i.e., a group of Pareto-optimal solutions) within a few hours, while other optimization algorithms tend to require a similar amount of computational time to acquire just a single Pareto-optimal trajectory.

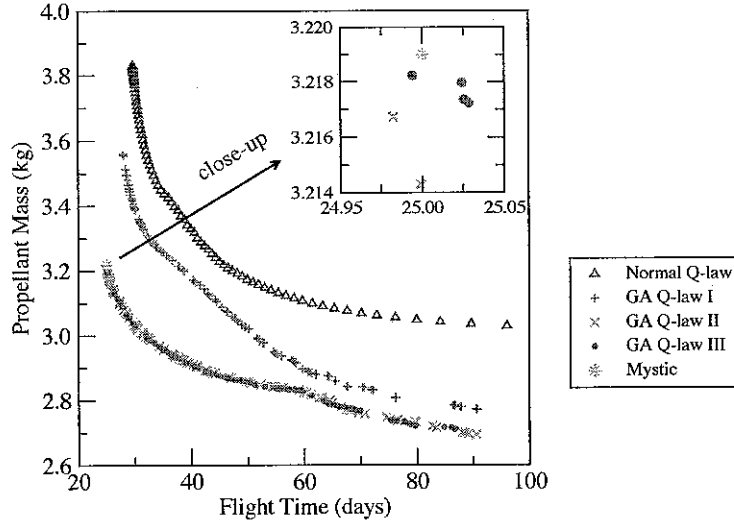


Figure 10. Case D: Trade-off between propellant mass and flight time. The Pareto front of the normal Q-law is obtained by varying $\eta_{\text{cut}} = [0, 1]$ and the initial true anomaly $\theta_i = [0, 2\pi]$. Three Pareto fronts of the GA optimized Q-law are generated as follows: the first Pareto front (GA Q-law I) is obtained by optimizing $\{W_a, W_e, W_i, W_\Omega, \eta_{\text{cut}}, \theta_i\}$, the second Pareto front (GA Q-law II) by optimizing $\{W_a, W_e, W_i, W_\Omega, \eta_{\text{cut}}, \theta_i, m, n, r\}$, and the third Pareto front (GA Q-law III) by optimizing $\{W_a, W_e, W_i, W_\Omega, \eta_{\text{cut}}, \theta_i, m, n, r, W_P, r_{p\text{min}}, k\}$. A Pareto-optimal solution found by Mystic is plotted for comparison.

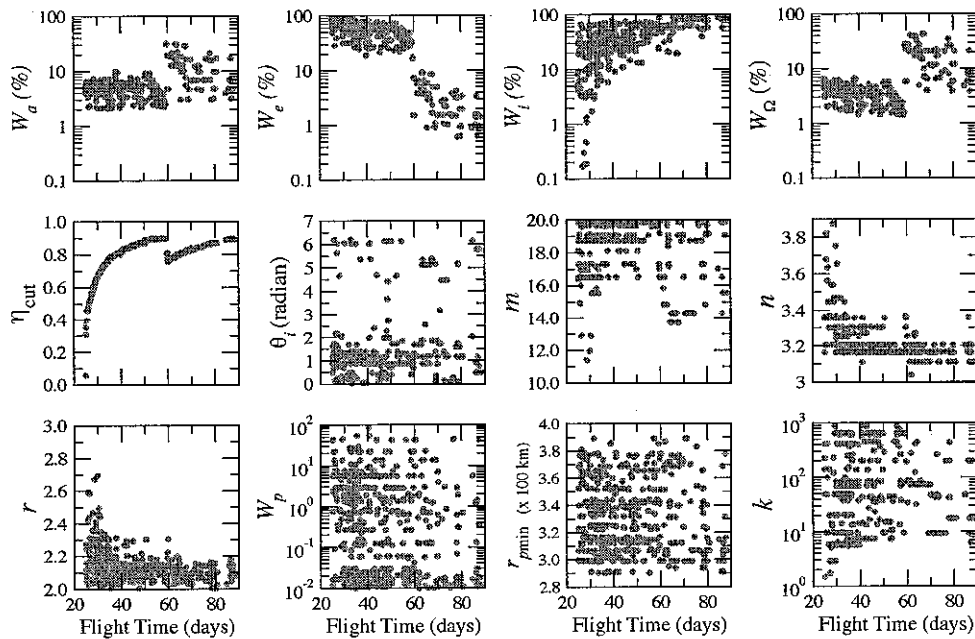


Figure 11. Case D: Optimal Q-law parameters found by GA with respect to flight time. The overall distribution of the optimal parameters shows that the Q-law performance is more sensitive to the choice of $\{W_a, W_e, W_i, W_\Omega, \eta_{\text{cut}}, \theta_i, m, n, r\}$ than $\{W_P, r_{p\text{min}}, k\}$. There is a strong correlation between η_{cut} and the flight time as shown in other transfer cases. However, the optimal η_{cut} shows a discontinuity around flight time 60 days, indicating a change of trajectory patterns. Optimal W_a, W_e, W_Ω also show a discontinuity around the flight time.

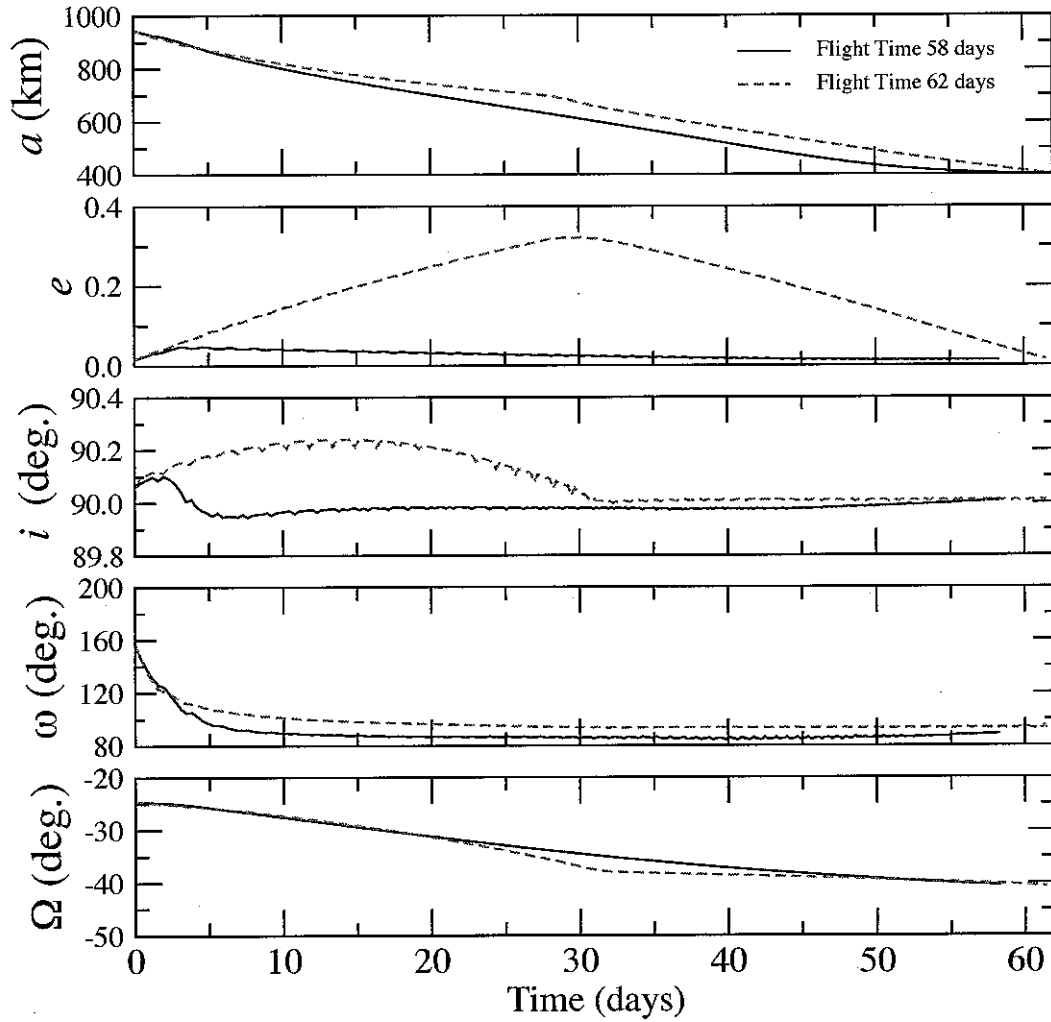


Figure 12. Case D: Orbit elements as a function of time for a Pareto-optimal trajectory with flight time 58 days (just below the discontinuity point of the optimal η_{cut} shown in Fig. 11) and one with flight time 62 days (just above the discontinuity point). A large difference in the time history of eccentricity between the two trajectories is shown, while other orbit elements show little difference.

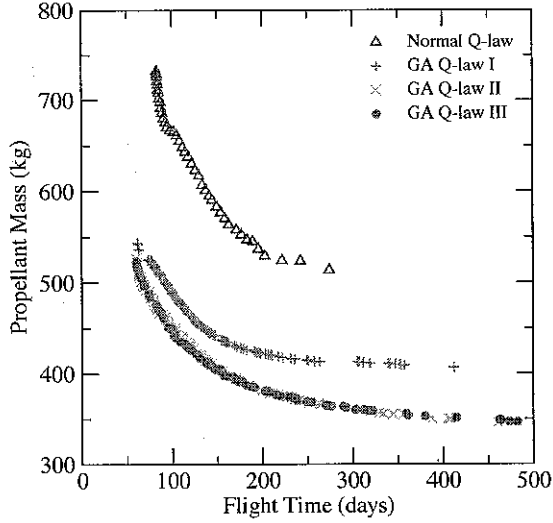


Figure 13. Case E: Trade-off between propellant mass and flight time. The Pareto front for the normal Q-law is obtained by varying $\eta_{cut} = [0, 1]$ and the initial true anomaly $\theta_i = [0, 2\pi]$. Three Pareto fronts for the GA optimized Q-law are generated as follows: the first Pareto front (GA Q-law I) by optimizing $\{W_a, W_e, W_i, W_\omega, W_\Omega, \eta_{cut}, \theta_i\}$, the second Pareto front (GA Q-law II) by optimizing $\{W_a, W_e, W_i, W_\omega, W_\Omega, \eta_{cut}, \theta_i, m, n, r\}$ and the third Pareto front (GA Q-law III) by optimizing $\{W_a, W_e, W_i, W_\omega, W_\Omega, \eta_{cut}, \theta_i, m, n, r, W_P, r_{pmin}, k\}$. The GA optimized Q-law provides a better estimation of the Pareto front than the normal Q-law for all the flight times considered. The propellant mass saving as much as 30% is obtained with the GA optimized Q-law.

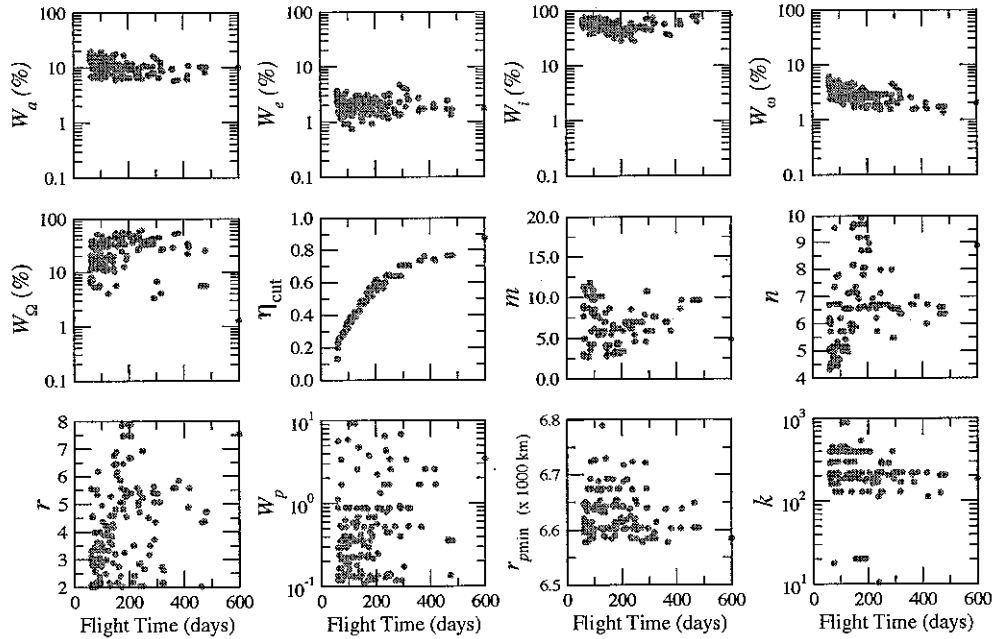


Figure 14. Case E: Optimal Q-law parameters found by GA with respect to flight time. There is a strong correlation between η_{cut} and the flight time, while other Q-law parameters show a weak correlation. A strong preference of small values of W_e/W_a and W_ω/W_a is observed, whereas a wide range of W_i/W_a and W_Ω/W_a values is found to be optimal.

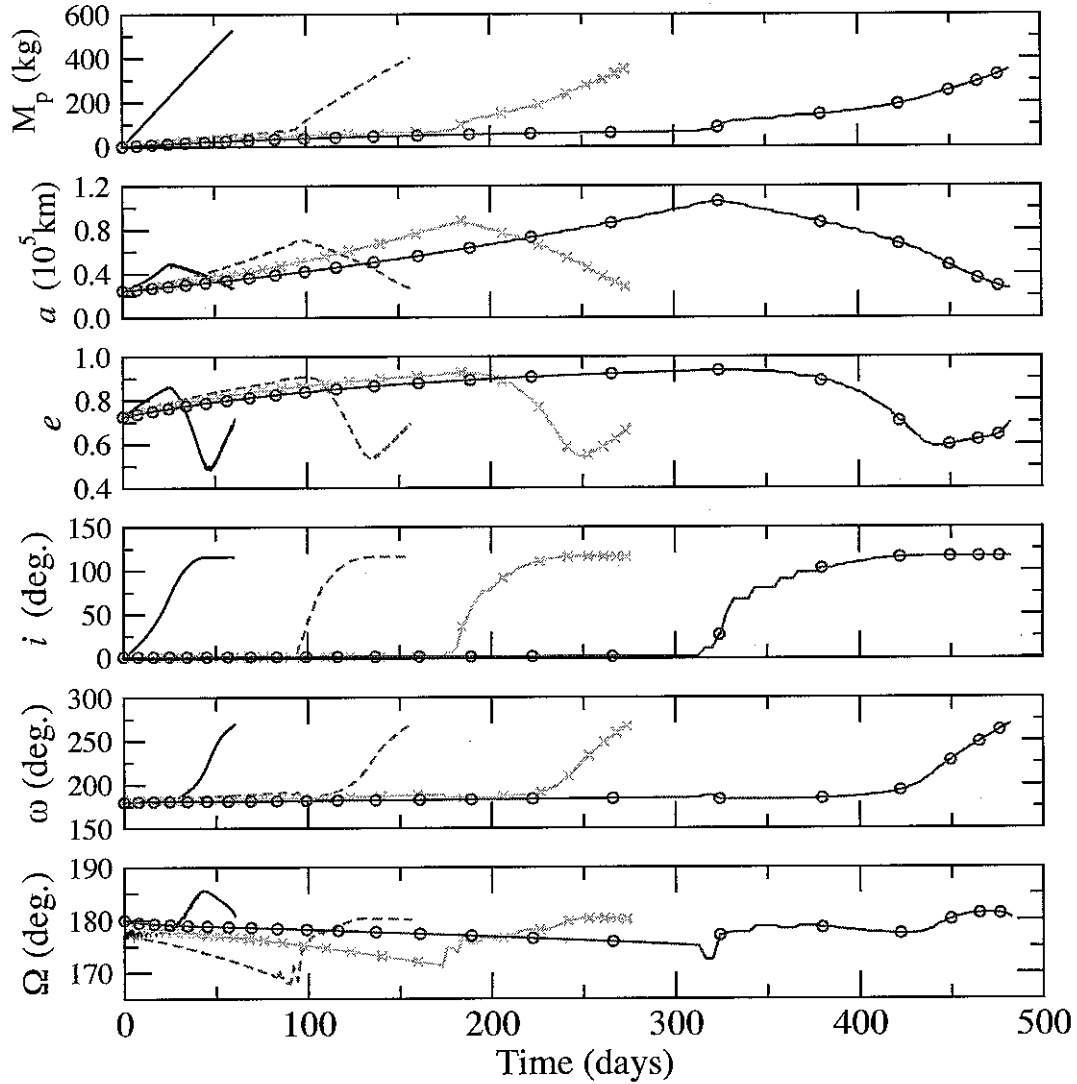


Figure 15. Case E: Consumed propellant mass and orbit elements as a function of time for four Pareto-optimal trajectories among the solutions found by GA Q-law III. The solid line is the trajectory with flight time 60 days, the dashed line is the trajectory with flight time 156 days, the line with x symbols is the trajectory with flight time 275 days, and the line with circles is the trajectory with flight time 482 days. As a general pattern, the trajectory with a longer flight time involves a larger change of semimajor axis and a later change of inclination.

5. CONCLUSIONS

For the design and optimization of trajectories powered by low-thrust propulsion, we have developed an efficacious and efficient method to obtain approximate propellant and flight-time requirements and Pareto-optimal trajectories. The method involves two-level optimizations: i) optimal thrust angles and locations are determined by the Q-law, ii) the Q-law is optimized with two evolutionary algorithms: a genetic algorithm and a simulated-annealing-related algorithm. We have applied our method to four different types of orbit transfers around the Earth and one orbit transfer around the asteroid Vesta. The resulting Pareto front with the optimized Q-law shows as much as a 30% savings of propellant in comparison with an unoptimized Q-law, and the Pareto front contains the optimal solutions found by other trajectory optimization algorithms.

In optimization problems, there is always a trade-off between the optimization quality and the computational requirement. Most of efficient (fast) optimization tools tend to yield low-quality solutions while high-quality optimization tools tend to demand high computational requirements. It is both decent quality of optimization and low computational requirement that are needed for the early stage of mission design where many possible scenarios are considered. Our method offers both the high optimization quality and the high computational efficiency. The trajectory quality of our method is shown to be as good as that of other available optimization tools. Our method provides not only a few Pareto-optimal trajectories but also a decent Pareto front for a given orbit transfer within a few hours of computation time. The computational efficiency arises from both the efficiency of the Q-law in obtaining a candidate trajectory and the easy parallelism of GA/SA computation involving the population of candidate Q-laws/trajectories.

6. ACKNOWLEDGMENTS

The authors thank Christoph Adami, Van Dang, and Didier Keymeulen for useful discussions. This work was performed at the Jet Propulsion Laboratory, California Institute of Technology under a contract with the National Aeronautics and Space Administration. The research was supported by JPL R&TD program.

7. APPENDIX

Mathematically, a multi-objective optimization problem is expressed as

$$\text{minimize } \mathbf{y} = \{y_1(\mathbf{x}), \dots, y_M(\mathbf{x})\} \in \mathbf{Y}, \quad (\text{A.1})$$

$$\text{where } \mathbf{x} = \{x_1, \dots, x_N\} \in \mathbf{X}, \quad (\text{A.2})$$

and \mathbf{x} is the N dimensional decision vector, \mathbf{y} the M dimensional objective vector, \mathbf{X} the decision space, and \mathbf{Y} the objective space.

Within the multi-objective optimized problem, a nondominated solution is the solution that is not dominated by any

other feasible solutions. The condition for the solution \mathbf{x}^a to dominate \mathbf{x}^b is given by

$$\begin{aligned} & \forall i \in \{1, \dots, M\}, y_i(\mathbf{x}^a) \leq y_i(\mathbf{x}^b) \\ \wedge & \exists i \in \{1, \dots, M\}, y_i(\mathbf{x}^a) < y_i(\mathbf{x}^b). \end{aligned} \quad (\text{A.3})$$

The second condition ensures that $\mathbf{y}(\mathbf{x}^a) \neq \mathbf{y}(\mathbf{x}^b)$.

REFERENCES

- [1] A.E. Petropoulos, "Simple Control Laws for Low-Thrust Orbit Transfers," *AAS/AIAA Astrodynamics Specialist Conference*, AAS Paper 03-630, 2003.
- [2] A.E. Petropoulos, "Low-Thrust Orbit Transfers Using Candidate Lyapunov Functions with a Mechanism for Coasting," *AIAA/AAS Astrodynamics Specialist Conference*, AIAA Paper 2004-5089, 2004.
- [3] J.H. Holland, *Adaptation in Natural and Artificial Systems*, The University of Michigan Press, Ann Arbor, Michigan, 1975.
- [4] A.H.F. Dias and J.A. de Vasconcelos, "Multiobjective Genetic Algorithms Applied to Solve Optimization Problems," *IEEE Trans. Magn.*, **38**, 1133–1136, 2002.
- [5] J.D. Schaffer, "Multiple Objective Optimization with Vector Evaluated Genetic Algorithms," Ph.D. thesis, Vanderbilt University, 1984.
- [6] J. Horn, N. Nafpliotis, and D.E. Goldberg, "A niched pareto genetic algorithm for multiobjective optimization," *Proc. 1st IEEE Conf. Evolutionary Computation*, **1**, 82–87, 1994.
- [7] C.M. Fonseca and P.J. Fleming, "Genetic algorithms for multiobjective optimization", *Proc. 5th Int. Conf. Genetic Algorithms*, 416–423, 1993.
- [8] Metropolis, N., Rosenbluth, A.W., Rosenbluth, M.N., Teller, A.H., Teller, E., "Equation of State Calculation by Fast Computing Machines," *J. of Chem. Phys.*, **21**, 1087–1091, 1953.
- [9] Kirkpatrick, S., Gelat, C.D., Vecchi, M.P., "Optimization by Simulated Annealing," *Science*, **220**, 671–680, 1983.
- [10] N. Srinivas and K. Deb, "Multiobjective optimization using nondominated sorting in genetic algorithms," *Evolutionary Computation*, **2**, 221–248, 1994.
- [11] T.N. Edelbaum, "Optimum Power-Limited Orbit Transfer in Strong Gravity Fields," *AIAA Journal*, **3**, 921–925, 1965.
- [12] S. Geffroy and R. Epenoy, "Optimal Low-Thrust Transfers with Constraints - Generalization of Averaging Techniques," *Astronautica Acta*, **41**, 133–149, 1997.
- [13] G.J. Whiffen and J. A. Sims, "Application of a Novel Optimal Control Algorithm to Low-Thrust Trajectory Optimization," *AAS/AIAA Space Flight Mechanics Meeting*, AAS Paper 01-209, 2001.

- [14] G.J. Whiffen, "Optimal Low-Thrust Orbit Transfers around a Rotating Non-Spherical Body" AAS/AIAA Space Flight Mechanics Meeting, AAS Paper 04-264, 2004.
- [15] The initial and final orbit of the Mystic solution are identical to our case D transfer. Mystic initially searched for an optimal trajectory to a different target orbit ($a=375$ km) while requiring the flight time to be smaller than 25 days. However, Mystic could not find a trajectory that can meet the flight time requirement. The Mystic solution compared here is the trajectory that ends up closest to the target orbit. To make a meaningful comparison, we set the final orbit of the Mystic solution as the target orbit of our case D transfer.

Richard Terrile created and leads the Evolutionary Computation Group at the Jet Propulsion Laboratory. His group has developed genetic-algorithm based tools to improve on human design of space systems and has demonstrated that computer-aided design tools can also be used for automating innovation and design of complex systems. He is an astronomer, the Mars Sample Return Study Scientist, the JIMO Deputy Project Scientist and the co-discoverer of the Beta Pictoris circumstellar disk. Dr. Terrile has B.S. degrees in Physics and Astronomy from the State University of New York at Stony Brook and an M.S. and a Ph.D. in Planetary Science from the California Institute of Technology in 1978.

BIOGRAPHY

Seungwon Lee is a member of technical staff at the Jet Propulsion Laboratory. Her research interest includes genetic algorithms, low-thrust trajectory design, nanoelectronics, quantum computation, parallel cluster computing, and advanced scientific software modernization techniques. Seungwon received her B.S. and M.S. in physics from the Seoul National University in 1997 and her Ph.D. in physics from the Ohio State University in 2002. Her work is documented in numerous journals and conference proceedings.

Paul von Allmen is the supervisor of the Applied Cluster Computing Technologies group and a senior researcher at the Jet Propulsion Laboratory. Paul is currently leading research in quantum computing, thermoelectric and nonlinear optics material and device design, nano-scale chemical sensors, semiconductor optical detectors, and low-thrust trajectory optimization. Prior to joining JPL in 2002, Paul worked at the IBM Zurich Research Lab on semiconductor diode lasers, at the University of Illinois on the silicon device sintering process, and at the Motorola Flat Panel Display Division as manager of the theory and simulation group and as principal scientist on micro-scale gas discharge UV lasers. Paul received his Ph.D. in physics from the Swiss Federal Institute of Technology in Lausanne, Switzerland in 1990. His work is documented in numerous publications and patents.

Wolfgang Fink is a Senior Researcher at NASA's Jet Propulsion Laboratory, Pasadena, CA, Visiting Research Assistant Professor of both Ophthalmology and Neurological Surgery at the University of Southern California, Los Angeles, CA, and Visiting Associate in Physics at the California Institute of Technology, Pasadena, CA. His research interests include theoretical and applied physics, biomedicine, astrobiology, computational field geology, and spacecraft/rover autonomy. He is the author over 16 articles and over 48 conference proceedings in the areas indicated above. Dr. Fink obtained an M.S. degree in physics from the University of Göttingen in 1993, and a Ph.D. in theoretical physics from the University of Tübingen in 1997.